Article:
Trugilho, L.F., Auer, S. orcid.org/0000-0003-0418-1745 and Rizzi, L.G. (2024) A density of states-based approach to determine temperature-dependent aggregation rates. The Journal of Chemical Physics, 161 (5). 051101. ISSN 0021-9606

https://doi.org/10.1063/5.0221950

A density of states-based approach to determine temperature-dependent aggregation rates

L. F. Trugilho,[1,2] S. Auer,[3] and L. G. Rizzi[2, a)]
[1)] *Faculty of Biological Sciences, University of Leeds, Leeds LS2 9JT, United Kingdom.*
[2)] *Departamento de Física, Universidade Federal de Viçosa (UFV), Av. P. H. Rolfs, s/n, 36570-900, Viçosa, Brazil.*
[3)] *School of Chemistry, University of Leeds, Leeds LS2 9JT, United Kingdom.*

Here we establish an approach to determine temperature-dependent aggregation rates in terms of thermostatistical quantities which can be obtained directly from flat-histogram and statistical temperature algorithms considering the density of states of the system. Our approach is validated through simulations of an Ising-like model with anisotropically interacting particles at temperatures close to its first-order phase transition. Quantitative comparisons between the numerically obtained forward and reverse rates to approximate analytical expressions corroborate its use as a model-independent approach.

Over the last three decades, the so-called flat-histogram algorithms like multicanonical[1], entropic sampling[2], broad histogram[3], Wang-Landau[4], and those based on statistical temperature[5,6], have been explored as powerful numerical tools in the study of phase transitions in finite systems[7,8]. One advantage is that such algorithms yield estimates for the system's density of states $\Omega(E)$ over a wide range of energies E, and, by knowing $\Omega(E)$, one can access any thermostatistical information about the system by means of its microcanonical entropy $S(E) = k_B \ln \Omega(E)$. In fact, one can obtain not only the usual thermodynamics quantities from $S(E)$, but it also provides a way to perform systematic analyses through the inflection points of its derivatives[9,10], *e.g.*, the microcanonical inverse temperature $b(E) = k_B^{-1}(dS/dE)_{N,V}$ and $\gamma(E) = (db(E)/dE)_{N,V}$.

While quantities obtained from $\Omega(E)$ have been routinely explored in equilibrium-related thermostatistics analyses[11–19], the possibility of using energy-dependent free-energy profiles (FEPs) in the assessment of phase change kinetics has been only recently considered in the literature[20]. As argued in Ref.[20], a kinetic approach based on FEPs would be of considerable interest in the study of aggregation in finite systems which display first-order phase transitions[21]. This because, in practice, assumptions based either on the capillarity approximation[22] or on an arbitrary shape for the aggregates have proven to be difficult to accommodate even for the simplest systems[23,24], *e.g.*, systems where the anisotropy in the particles' interaction leads to the formation of filament-like aggregates.

Besides the attempts carried out in Ref.[20] to estimate rates from energy-based FEPs, additional efforts have been made in Refs.[25,26]. Although the authors in Ref.[20] considered distinct three-dimensional systems with either Lennard-Jones particles or polymer chains, they included estimates for the aggregation rates only at the transition temperature. In Ref.[26], on the other hand, approximated temperature-dependent expressions were introduced, but their quantitative agreement with the numerically obtained rates was assessed only for one-dimensional Markovian models. Since the kinetics of collective coordinates projected from a highly dimensional space, such as the energy E, is expected to be non-Markovian[27,28], reliable procedures for the evaluation of temperature-dependent rates for more detailed systems and comprehensive simulations have yet to be developed. Hence, here we perform simulations using a two-dimensional Ising-like model with anisotropically interacting particles[23,24,29,30]. Then, for comparison, we evaluate the forward and reverse rates near the transition temperature of its phase transition via different procedures, including the one based on $\Omega(E)$.

The model consists of N particles that can be in any of the $L \times L$ sites of a square lattice with periodic boundary conditions. In particular, we assume $L = 200$ and $N = 400$ so that the system has a constant concentration $\rho = N/L^2 = 10^{-2}$. Aligned nearest-neighbor (NN) particles interact through a stronger effective interaction denoted by ψ_s, while non-aligned NN particles present an effective interaction strength given by ψ_w, so that the anisotropy of the interaction is given by $\xi = \psi_s/\psi_w$. Although Monte Carlo (MC) simulations do not necessarily reproduce real diffusive dynamics, there is evidence that it could be used to describe it as long as only physical movements are considered[31,32]. Hence, diffusive-like dynamics are implemented in the model through local Kawasaki movements[33] where the particles can move only to their unoccupied NN sites. Each time step corresponds to one MC sweep where N attempts are made to rotate and move selected particles to one of their randomly selected NN sites.

Before discussing the aggregation kinetics, we include in Fig. 1 the equilibrium free-energy profiles, *i.e.*, FEPs, $\beta^* \Delta F(E)$, which were computed from the microcanonical entropies $S(E)$. Here, the microcanonical entropies $S(E)$ were numerically evaluated through the recursion steps of the multicanonical algorithm[34,35], where we considered $N_r = 500$ recursion steps with $N_s = 10^6$ MC sweeps each. As discussed in Refs.[26,36], the FEPs can be obtained as $\beta^* \Delta F(E) = (S^*(E) - S(E))/k_B$, where

[a)] Electronic mail: `lerizzi@ufv.br` (Corresponding author)

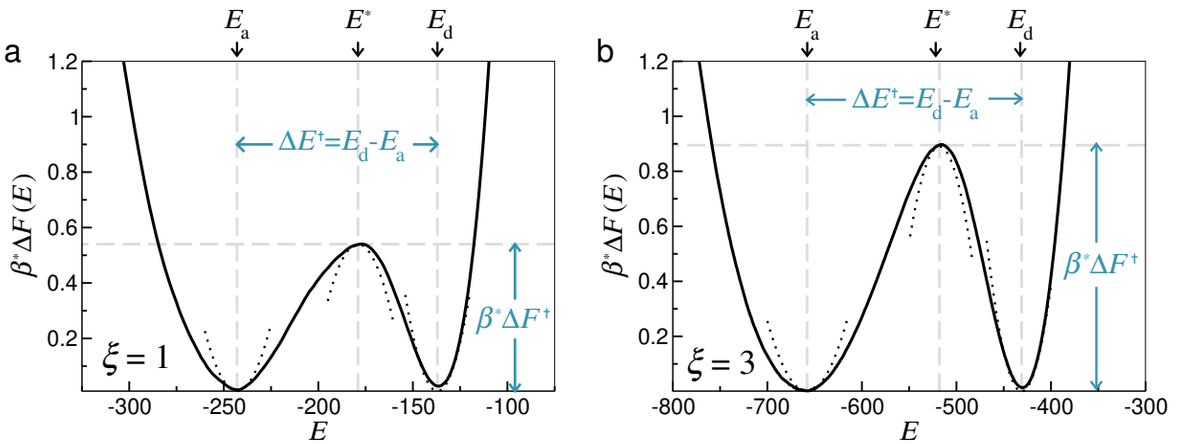

FIG. 1. Free-energy profiles, *i.e.*, FEPs, $\beta^*\Delta F(E)$ obtained for both (a) isotropic and (b) anisotropic cases. Free-energy barriers and latent heats are indicated by $\beta^*\Delta F^\dagger$ and $\Delta E^\dagger = E_d - E_a$, respectively, while $\Delta E_a^\ddagger = E^* - E_a$ and $\Delta E_d^\ddagger = E^* - E_d$ denote energy differences as defined in Eqs. 1 and 2. Dotted lines correspond to quadratic functions near the maxima and the minima of the FEPs, that is, $\beta^*\Delta F(E) \approx \beta^*\Delta F^\dagger - (\gamma^*/2)(E - E^*)^2$ and $\beta^*\Delta F(E) \approx (\gamma_{a(d)}/2)(E - E_{a(d)})^2$. Here, to illustrate their suitability, the parameters γ^*, γ_a, and γ_d were determined from the numerical data displayed in Fig. 2 (see also Table I).

$S^*(E) = k_B\beta^*(E - E_a) + S(E_a)$, with E_a being the lowest energy where the FEP has a minimum, and $\beta^* = 1/k_BT^*$, with T^* being the transition temperature determined through a Maxwell-like construction[25,26,30,36] and which separates the aggregated and the diluted phases (here denoted by the subscripts "a" and "d", respectively). As is seen in Fig. 1, such free-energy profiles are characterized by both their barrier height $\beta^*\Delta F^\dagger$ and latent heat $\Delta E^\dagger$. In addition, the asymmetry of the free-energy profiles can be characterized by the energy differences $\Delta E_a^\ddagger = E^* - E_a$ and $\Delta E_d^\ddagger = E^* - E_d$, as well as by curvature-related parameters that are evaluated around the maximum and the minima of the FEPs, which are given by $\gamma^* = (db(E)/dE)|_{E=E^*} > 0$ and $\gamma_{a(d)} = -(db(E)/dE)|_{E=E_{a(d)}} > 0$ (see the caption of Fig. 1). The results in Fig. 1 show that the values of both $\beta^*\Delta F^\dagger$ and $\Delta E^\dagger$ are higher for the anisotropic case where $\xi = 3$. Here we include results for these two values of ξ to illustrate the difference between the cases of a very low barrier (*i.e.*, the isotropic case with $\xi = 1$), and a case which should be representative of systems with higher barriers (*i.e.*, the anisotropic case with $\xi = 3$). Nonetheless, it is worth noting that, for this model, the behavior of the free-energy barrier is non-monotonic as a function of the anisotropy[30].

Now we change our attention to the kinetic aspects of the transition. In contrast to the multicanonical simulations used to determine $S(E)$, for the data production runs the system is assumed to be in contact with an implicit thermal bath at a specific temperature T so the simulations are carried out in the NVT ensemble via the usual Metropolis algorithm[33]. One should note that near the transition temperature $T^* = 1/k_B\beta^*$, the system makes transitions between the diluted and the aggregated phases. Hence, for each temperature, one can estimate temperature-dependent rates as $\kappa_a = 1/\tau_{d\to a}$ and $\kappa_d = 1/\tau_{a\to d}$, where $\tau_{a\to d}$ and $\tau_{d\to a}$ correspond to the mean first passage times (MFPTs), here evaluated directly from the energy time series using the method of labeled walkers described in Ref.[37] (see also Ref.[25]). In order to perform such estimates at each given temperature $T = 1/k_B\beta$, we initiate the system's configuration with randomly placed and oriented particles at the dilute phase, and the analysis starts once the first transition between energies E_a and E_d is completed, then we compute the MFPTs between these two energies with at least 10^2 roundtrips[37]. Figure 2 shows results for the temperature-dependent rates for both the isotropic ($\xi = 1$) and the anisotropic ($\xi = 3$) cases. One striking feature which is common to both cases is that the rates κ_a and κ_d do display a non-Arrhenius behavior, even though the equilibrium constants κ_{eq} seem to be linear in a mono-log plot (*i.e.*, similar to the usually observed van't Hoff's behavior).

As discussed in Refs.[25,26], one has that, near the transition temperature, the forward and the reverse rates can be estimated, respectively, as

$$\kappa_a = \frac{1}{\tau_{d\to a}} \approx A_d \exp\left[-\Delta E_d^\ddagger(\beta - \beta^*) - \frac{\bar\gamma_d}{2}(\beta - \beta^*)^2\right] , \quad (1)$$

and

$$\kappa_d = \frac{1}{\tau_{a\to d}} \approx A_a \exp\left[-\Delta E_a^\ddagger(\beta - \beta^*) - \frac{\bar\gamma_a}{2}(\beta - \beta^*)^2\right] , \quad (2)$$

where $\Delta E_{a(d)}^\ddagger = E^* - E_{a(d)}$ and $\bar\gamma_{a(d)} = (\gamma_{a(d)})^{-1} + (\gamma^*)^{-1}$. In addition, these two rates can be used to eval-

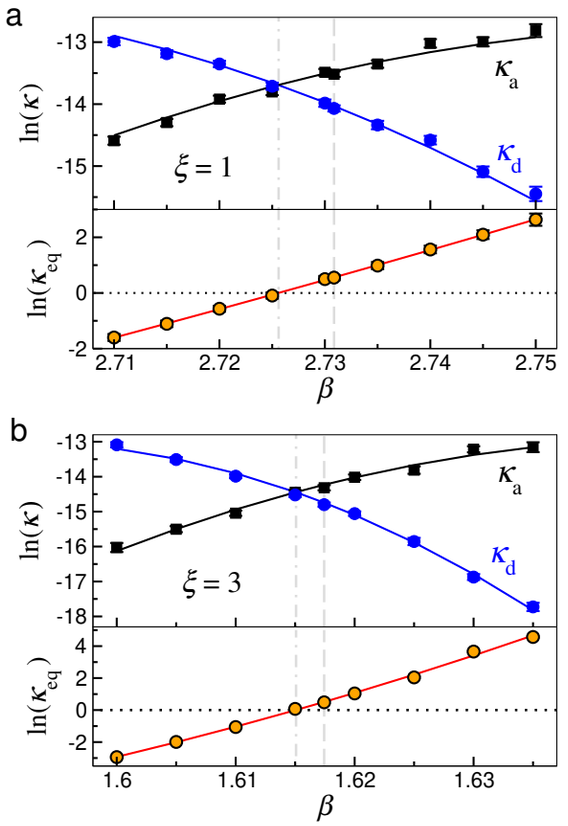

FIG. 2. Temperature-dependent rates $\kappa_{\rm a}$, $\kappa_{\rm d}$, and the equilibrium constant $\kappa_{\rm eq}$ for both (a) isotropic and (b) anisotropic cases. Symbols denote results determined numerically from the MFPTs obtained from the energy time series, while continuous lines correspond to the fit of Eqs. 1, 2, and 3 to the numerical data. Numerical fits were done with the pre-factors defined by Eq. 4 in (a) and Eq. 5 in (b). Vertical dashed and dash-dotted (grey) lines indicate the inverse of the temperatures β^* and β_m, respectively.

uate the equilibrium constant as

$$\kappa_{\rm eq} = \frac{\kappa_{\rm a}}{\kappa_{\rm d}} \approx A \exp\left[\Delta E^{\ddagger}(\beta-\beta^*) + \frac{\Delta\bar{\gamma}}{2}(\beta-\beta^*)^2\right] \quad . \tag{3}$$

where $\Delta\bar{\gamma} = \bar{\gamma}_{\rm a} - \bar{\gamma}_{\rm d} = (\gamma_{\rm a})^{-1} - (\gamma_{\rm d})^{-1}$ and $\Delta E^{\ddagger} = E_{\rm d} - E_{\rm a}$. It is worth noting that the pre-factors in the above expressions are slightly different depending on the relative intensity of the free-energy barrier. For low barriers, one has that[25]

$$A_{\rm a(d)} = (D^*/|\Delta E^{\ddagger}_{\rm a(d)}|)\sqrt{\gamma^*/(2\pi)}e^{-\beta^*\Delta F^{\dagger}} \quad , \tag{4}$$

so that $A = |\Delta E^{\ddagger}_{\rm a}|/|\Delta E^{\ddagger}_{\rm d}|$, while for higher free-energy barriers one should use a Kramers-like approximation[26] and the pre-factors are instead given by

$$A_{\rm a(d)} = (D^*/2\pi)\sqrt{\gamma^*\gamma_{\rm a(d)}}\, e^{-\beta^*\Delta F^{\dagger}} \quad , \tag{5}$$

so that $A = \sqrt{\gamma_{\rm d}/\gamma_{\rm a}}$ (*i.e.*, in either case the pre-factor of the equilibrium constant $\kappa_{\rm eq}$ is given by $A = A_{\rm a}/A_{\rm d}$).

One should note that, except for the value of D^*, which corresponds to a diffusion coefficient related to the random walk of the system in the projected energy space, all other quantities can be estimated directly from the free-energy profiles $\beta^*\Delta F(E)$ displayed in Fig. 1.

In order to get an estimate for D^*, we consider the function $Z_{C,1}$ that is related to the cut-based free-energy profiles of generalized reaction coordinates[27,38]. For a given sampling interval $\Delta t_k = k\Delta t_0$ and using the energy E as a reaction coordinate, it can be computed as[27]

$$Z_{C,1}(E;\Delta t_k) = \frac{1}{2}{\sum_i}' |E((i+1)\Delta t_k) - E(i\Delta t_k)| \ , \tag{6}$$

where the prime indicates that the sum is performed over all i that E is in between the values $E(i\Delta t_k)$ and $E((i+1)\Delta t_k)$ taken at "successive" time steps[39]. As discussed in Ref.[38], $Z_{C,1}(E;\Delta t_k)$ can be related to the mean-squared displacement of the reaction coordinate, thus one can use it to estimate the energy- and time-dependent diffusion coefficient numerically as

$$D(E;\Delta t_k) = \frac{Z_{C,1}(E;\Delta t_k)}{\Delta t_k\, H(E;\Delta t_k)} \quad , \tag{7}$$

where $H(E;\Delta t_k)$ is the usual (non-normalized) histogram obtained from the energy series with the sampling interval Δt_k. In addition, since Eqs. 1 and 2 assume an effective energy-independent diffusion coefficient, we also evaluate the following average

$$D(\Delta t_k) = \int_{E_{\rm a}}^{E_{\rm d}} D(E;\Delta t_k) p^*(E) dE \quad , \tag{8}$$

where $p^*(E)$ is the equilibrium distribution at T^*, and is related to the FEP as $p^*(E) \propto e^{-\beta^*\Delta F(E)}$. In Fig. 3 we display the time-dependent diffusion coefficient given by Eq. 8 for both the isotropic and anisotropic cases. Accordingly, $D(\Delta t_k)$ becomes almost constant for large k, indicating that the dynamics of the projected energy coordinate are nearly diffusive at large time scales, so for each case, we took the corresponding limiting value of it as the proper estimate for the effective parameter D^*.

We note that, since the diffusion coefficient $D(\Delta t_k)$ changes with Δt_k for small k, *i.e.*, it displays a subdiffusive behavior with powerlaw exponents around -0.5 and -0.6, one can infer from the results shown in Fig. 3 that $Z_{C,1}(E;\Delta t_k)$ may also depend on the sampling interval (*i.e.*, the dependence on Δt_k of the histogram, $H \sim \Delta t_k^{-1}$, cancels out with Δt_k in Eq. 7). The dependence of both $D(\Delta t_k)$ and $Z_{C,1}$ on Δt_k (data not shown) strongly suggests that, at short time scales, the dynamics of the projected coordinate E is non-Markovian[27]. This result agrees with the general behavior expected from Ref.[40], which asserts that the self-assembly of particles that follow deterministic Newtonian dynamics is not a Markovian process. Hence, although the numerical approach considered here assumes diffusive-like motion for the interacting particles, our simulations achieved

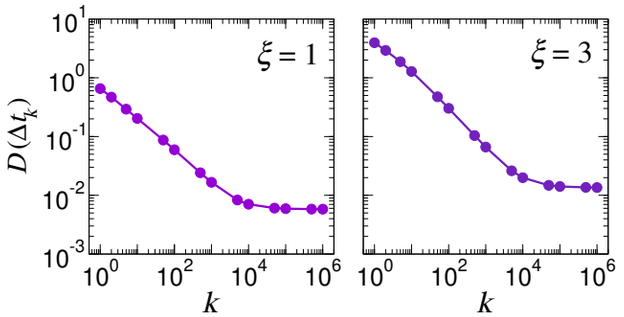

FIG. 3. Diffusion coefficient $D(\Delta t_k)$ given by Eq. 8 as a function of the sampling index k with $\Delta t_0 = 20\,\mathrm{MCs}$ for both (a) isotropic and (b) anisotropic cases. The limiting values of $D(\Delta t_k)$ at large k correspond to $D^* = 0.0058$ and $D^* = 0.0136$ for $\xi = 1$ and $\xi = 3$, respectively.

their purpose in obtaining a projected reaction coordinate which has physically admissible dynamics.

Now, by imposing the values obtained for D^* from Fig. 3 and the values for β^* and for the free-energy barrier $\beta^*\Delta F^\dagger$ determined from Fig. 1, but allowing the energy differences $\Delta E^\ddagger_{\mathrm{a(d)}}$ and the curvature-related parameters, *i.e.*, γ^*, γ_a, and γ_d, to act as free parameters, we are able to examine the fit of Eqs. 1, 2, and 3 to the numerical data presented in Fig. 2. Remarkably, given the approximated character of those expressions, Table I indicates a fair agreement between the values directly determined from the free-energy profiles displayed in Fig. 1 and the values indirectly obtained from the numerical fits shown in Fig. 2. Evidently, the free-energy profiles are not perfectly quadratic functions near their extrema, so the evaluation of the curvature-related parameters is not precise (*i.e.*, it depends on how far from the extrema one considers the fit to the data). However, as one can see from the dotted lines displayed in Fig. 1, the values determined from the kinetic data lead to an acceptable description of the FEPs, even though the values of γ^*, γ_a, and γ_d are slightly different from the best values that were directly extracted from the FEPs (see Table I).

The results displayed in Fig. 1 for both $\xi = 1$ and $\xi = 3$ indicate that $\gamma_\mathrm{d} > \gamma_\mathrm{a}$, which means that the valleys related to the diluted state are narrower than the ones associated with the aggregated state. In a broad sense, the validation of Eqs. 1, 2, and 3 suggests that the values obtained for their parameters may help one to describe equilibrium free-energy profiles from kinetic data. Conversely, estimates for the rates could be readily obtained from the FEPs, and that may be widely explored since flat-histogram algorithms[1–4] have been extensively used to determine the microcanonical entropy $S(E)$ in finite systems with first-order phase transitions[11–13]. In those cases, it is worth noting that β^* is related to the temperature T^* where the depths of the valleys of the FEP are equal, but, with the exception of the cases of fully symmetric FEPs, where the widths and curvatures of the valleys are identical, that will be not the same as

TABLE I. Parameters obtained both directly from the FEPs displayed in Fig. 1, and indirectly from the fits of Eqs. 1, 2, and 3, to the numerical data presented in Fig 2.

	$\xi = 1$		$\xi = 3$	
	from FEP	from fit	from FEP	from fit
$\beta^*\Delta F^\dagger$	0.53	–	0.88	–
β^*	2.73087	–	1.61744	–
$\Delta E^\ddagger$	106	107	227	217
$\Delta E^\ddagger_a$	64	68	140	132
$\Delta E^\ddagger_d$	−42	−39	−87	−85
γ^*	0.7×10^{-3}	1.6×10^{-3}	4.0×10^{-4}	6.8×10^{-4}
γ_a	0.8×10^{-3}	1.5×10^{-3}	1.5×10^{-4}	2.9×10^{-4}
γ_d	2.0×10^{-3}	2.4×10^{-3}	7.2×10^{-4}	8.0×10^{-4}

the temperature $T_m = 1/k_B\beta_m$ where $\kappa_\mathrm{eq} = 1$, that is, where $\kappa_\mathrm{a} = \kappa_\mathrm{d}$. As discussed in Refs.[25,26], the temperature T_m is related to the situation where the phases have the same steady-state probability, *i.e.*, equal area criteria. Nevertheless, one can show that the two temperatures are related to each other as $\beta_m = \beta^* + \delta$, where the correction factor is either $\delta = |\Delta E^\ddagger|^{-1} \ln|\Delta E^\ddagger_\mathrm{d}/\Delta E^\ddagger_\mathrm{a}|$ if the free-energy barrier is small[25], or $\delta = (2|\Delta E^\ddagger|)^{-1} \ln(\gamma_\mathrm{a}/\gamma_\mathrm{d})$, for higher free-energy barriers[26]. The relationships between these temperatures are indeed corroborated by the numerical results presented in Fig. 2 for both $\xi = 1$ and $\xi = 3$. Accordingly, as Ref.[30] indicates, the latent heat increases linearly with L for the different anisotropies, so one may expect that the correction factor goes to zero as $\delta \approx L^{-1}$ at the thermodynamic limit, where one should have $\beta^* \approx \beta_m$.

Finally, it is worth mentioning that the numerical procedures as well as the equations that were examined here are model-independent, so it is straightforward to apply them to the description of the aggregation kinetics in more detailed systems which exhibit first-order phase transitions. These may include not only more realistic systems which display, *e.g.*, the aggregation of peptide chains[41] but also those with charged macromolecules[42], which have been hardly considered in the literature, in part, because of the limitations of the existing approaches when competing long-range interactions are present in the system.

The authors thank the funding agencies FAPEMIG, CNPq (312999/2021-6), and CAPES (PDSE program).

Author declarations

Conflict of Interest: The authors have no conflicts to disclose.

Data availability: The data that support the findings of this study are available from the corresponding author upon reasonable request.

References

[1] B. A. Berg and T. Neuhaus, Phys. Rev. Lett. **68**, 9 (1992).
[2] J. Lee, Phys. Rev. Lett. **71**, 211 (1993).
[3] P. M. C. de Oliveira, T. J. P. Penna, and H. J. Herrmann, Braz. J. Phys. **26**, 677 (1996).

[4]F. Wang and D. P. Landau, Phys. Rev. Lett. **86**, 2050 (2001).
[5]J. Kim, J. E. Straub, and T. Keyes, Phys. Rev. Lett. **97**, 050601 (2006).
[6]J. Kim, T. Keyes, and J. E. Straub, J. Chem. Phys. **135**, 061103 (2011).
[7]W. Janke, ed., *Rugged Free Energy Landscapes* (Springer, 2008).
[8]W. Janke and W. Paul, Soft Matter **12**, 642 (2016).
[9]S. Schnabel, D. T. Seaton, D. P. Landau, and M. Bachmann, Phys. Rev. E **84**, 011127 (2011).
[10]K. Qi and M. Bachmann, Phys. Rev. Lett. **120**, 180601 (2018).
[11]C. Junghans, M. Bachmann, and W. Janke, Phys. Rev. Lett. **97**, 218103 (2006).
[12]C. Junghans, M. Bachmann, and W. Janke, J. Chem. Phys. **128**, 085103 (2008).
[13]C. Junghans, M. Bachmann, and W. Janke, Europhys. Lett. **87**, 40002 (2009).
[14]J. Hernández-Rojas and J. M. Gomez Llorente, Phys. Rev. Lett. **100**, 258104 (2008).
[15]T. Chen, X. Lin, Y. Liu, and H. Liang, Phys. Rev. E **76**, 046110 (2007).
[16]T. Chen, X. Lin, Y. Liu, T. Lu, and H. Liang, Phys. Rev. E **78**, 056101 (2008).
[17]R. B. Frigori, L. G. Rizzi, and N. A. Alves, J. Chem. Phys. **138**, 015102 (2013).
[18]N. A. Alves, L. D. Morero, and L. G. Rizzi, Comput. Phys. Commun. **191**, 125 (2015).
[19]L. G. Rizzi and N. A. Alves, Phys. Rev. Lett. **117**, 239601 (2016).
[20]J. Zierenberg, P. Schierz, and W. Janke, Nat. Commun. **8**, 14546 (2017).
[21]J. Lee and J. M. Kosterlitz, Phys. Rev. Lett. **65**, 137 (1990).
[22]J. Merikanto, E. Zapadinsky, A. Lauri, and H. Vehkamäki, Phys. Rev. Lett. **98**, 145702 (2007).
[23]R. Cabriolu, D. Kashchiev, and S. Auer, J. Chem. Phys. **137**, 204903 (2012).
[24]R. J. Bingham, L. G. Rizzi, R. Cabriolu, and S. Auer, J. Chem. Phys. **139**, 241101 (2013).
[25]L. G. Rizzi, J. Stat. Mech. **2020**, 083204 (2020).
[26]L. F. Trugilho and L. G. Rizzi, Eur. Phys. Lett. (EPL) **137**, 57001 (2022).
[27]S. V. Krivov, J. Chem. Theory Comput. **9**, 135 (2013).
[28]W. Nadler and U. H. E. Hansmann, Phys. Rev. E **75**, 026109 (2007).
[29]J. Zhang and M. Muthukumar, J. Chem. Phys. **130**, 035102 (2009).
[30]L. F. Trugilho and L. G. Rizzi, J. Phys.: Conf. Ser. **1483**, 012011 (2020).
[31]E. Sanz and D. Marenduzzo, J. Chem. Phys. **132**, 194102 (2010).
[32]F. Müller, H. Christiansen, and W. Janke, Phys. Rev. Lett. **129**, 240601 (2022).
[33]D. P. Landau and K. Binder, *A Guide to Monte Carlo Simulations in Statistical Physics* (Cambridge University Press, 2000).
[34]B. A. Berg, Comput. Phys. Commun. **153**, 397 (2003).
[35]L. G. Rizzi and N. A. Alves, J. Chem. Phys. **135**, 141101 (2011).
[36]L. F. Trugilho and L. G. Rizzi, J. Stat. Phys. **186**, 40 (2022).
[37]S. Trebst, D. A. Huse, and M. Troyer, Phys. Rev. E **70**, 046701 (2004).
[38]S. V. Krivov, J. Phys. Chem. B **115**, 11382 (2011).
[39]When calculating $Z_{C,1}$ for large sampling intervals it is necessary to use the transition path segments rather than the trajectory itself, otherwise some transitions from one boundary to another will be undetected due to the low time resolution, resulting in slower kinetics[27].
[40]A. Kuhnhold, H. Meyer, G. Amati, P. Pelagejcev, and T. Schilling, Phys. Rev. E **100**, 052140 (2019).
[41]Y. Wang, S. J. Bunce, S. E. Radford, A. J. Wilson, S. Auer, and C. K. Hall, Proc. Natl. Acad. Sci. USA **116**, 2091 (2019).
[42]M. Muthukumar, *Physics of Charged Macromolecules* (Cambridge University Press, 2023).